RESEARCH

Host starvation and in hospite degradation of algal symbionts shape the heat stress response of the *Cassiopea*-Symbiodiniaceae symbiosis

Gaëlle Toullec[1]* , Nils Rädecker[1] , Claudia Pogoreutz[1,2] , Guilhem Banc-Prandi[1] , Stéphane Escrig[1], Christel Genoud[3] , Cristina Martin Olmos[1,4] , Jorge Spangenberg[5] and Anders Meibom[1,4]*

Abstract

Background Global warming is causing large-scale disruption of cnidarian-Symbiodiniaceae symbioses fundamental to major marine ecosystems, such as coral reefs. However, the mechanisms by which heat stress perturbs these symbiotic partnerships remain poorly understood. In this context, the upside-down jellyfish *Cassiopea* has emerged as a powerful experimental model system.

Results We combined a controlled heat stress experiment with isotope labeling and correlative SEM-NanoSIMS imaging to show that host starvation is a central component in the chain of events that ultimately leads to the collapse of the *Cassiopea* holobiont. Heat stress caused an increase in catabolic activity and a depletion of carbon reserves in the unfed host, concurrent with a reduction in the supply of photosynthates from its algal symbionts. This state of host starvation was accompanied by pronounced in hospite degradation of algal symbionts, which may be a distinct feature of the heat stress response of *Cassiopea*. Interestingly, this loss of symbionts by degradation was concealed by body shrinkage of the starving animals, resulting in what could be referred to as "invisible" bleaching.

Conclusions Overall, our study highlights the importance of the nutritional status in the heat stress response of the *Cassiopea* holobiont. Compared with other symbiotic cnidarians, the large mesoglea of *Cassiopea*, with its structural sugar and protein content, may constitute an energy reservoir capable of delaying starvation. It seems plausible that this anatomical feature at least partly contributes to the relatively high stress tolerance of these animals in rapidly warming oceans.

Keywords Climate change, Photosymbiosis, Cnidaria, Symbiodiniaceae, Bleaching, Metabolism, NanoSIMS

*Correspondence:
Gaëlle Toullec
gaelletoullec00@gmail.com
Anders Meibom
anders.meibom@epfl.ch
Full list of author information is available at the end of the article

Introduction

The immense diversity and prevalence of photosymbioses between cnidarian animal hosts and their intracellular dinoflagellate algal symbionts is testimony to their ecological success in the (sub-)tropical oceans of today [1, 2]. In these cnidarian-algal symbioses, algal symbionts fix large amounts of inorganic carbon through photosynthesis and subsequently transfer a substantial proportion of their photosynthates to their host [3–7]. This efficient transfer of photosynthate fuels the energy metabolism of the cnidarian host and can be sufficient to cover its respiratory carbon requirements [8]. In turn, the cnidarian host supplies the algal symbionts with inorganic nutrients from its own metabolism, CO_2 in particular [9, 10]. This efficient recycling of organic and inorganic nutrients enables the cnidarian-algal symbioses to thrive even in highly oligotrophic tropical environments [11].

Yet, this ecological success is threatened by global climate change, especially global warming [12]. Severe and prolonged heat stress can disturb this symbiosis, ultimately resulting in its breakdown [13, 14]. This susceptibility is particularly apparent in the coral-algal symbiosis that has constituted the functional basis of coral reef ecosystems over hundreds of millions of years [2, 15, 16]. The breakdown of this symbiosis due to heat stress, referred to as coral bleaching, results in the loss of algal symbiont cells and photosynthetic pigments, which makes the coral tissues appear transparent revealing the underlying white calcium carbonate skeleton [17]. During prolonged heat stress, bleaching thus deprives the host of its primary energy source, the algal photosynthates, typically resulting in starvation and, ultimately, death. Indeed, repeated mass bleaching events have caused mass mortality of corals in the last decades, pushing many coral reefs to the brink of ecological collapse [14, 18–20].

The breakdown of the cnidarian-algal symbiosis is not only the result of the thermal tolerance limits of either symbiotic partner but depends also on their interactions [21, 22]. In this context, recent studies have shown that the destabilization of symbiotic nutrient exchange precedes the breakdown of the coral-algal symbiosis during heat stress [23–26]. It has also been established that heterotrophic feeding enhances the tolerance and/or resilience of the coral-algae symbiosis to heat stress [27–29]. Hence, the heat tolerance of these animals appears to be intimately linked to the nutritional status of the host. However, the role of nutrient cycling and the nutritional state of symbiotic partners in the breakdown of cnidarian-algal symbiosis during heat stress remains poorly documented and understood.

Cassiopea, a genus of symbiotic jellyfish (Schyphozoa, Rhizostomae), is an emerging model organism for the study of cnidarian-algal symbiosis [30–32]. Similar to corals, *Cassiopea* is associated with dinoflagellates of the family Symbiodiniaceae. However, in contrast to corals and sea anemones where algal symbionts are harbored in host gastrodermal cells, *Cassiopea* medusae primarily host their symbionts in amoebocyte cells within the mesoglea [33, 34]. From within these amoebocytes, the algae support the anabolic growth of medusae by providing them with photosynthates [6, 33, 35–37], likely in the form of glucose, lipids, and amino acids [1, 38]. In contrast to corals, however, *Cassiopea* appears to thrive even under rapidly changing environmental conditions and some species have recently been described as invasive in many (sub-)tropical regions [39–42]. Similar to some non-symbiotic scyphozoan jellyfish [43], *Cassiopea* is considered to be relatively heat tolerant. Experiments suggest that loss of pigmentation in *Cassiopea* medusae occurs at higher temperatures than in most reef-building corals [44–49]. Moreover, a very limited number of bleaching events in nature have been reported for *Cassiopea* in the literature [50]. In part because of this relatively high heat tolerance and high trophic plasticity, *Cassiopea* is expected to become an ecological "winner" in increasingly anthropogenically altered marine environments, exhibiting marked increases in abundance and expansion of their distribution range [44, 46, 47, 49, 51–53].

Disentangling the key processes in the heat stress response of *Cassiopea* would provide important insights into the ecological success of this invasive jellyfish and improve our conceptual understanding of the mechanisms underlying thermal tolerance in cnidarian-algal symbioses in general. Specifically, we hypothesize that the nutrient status of symbiotic partners and their interaction are crucial drivers of the heat stress response of *Cassiopea* holobiont thereby resembling processes found in other photosymbiotic Cnidaria such as reef-building corals. Here we aimed to investigate the physiological, bioenergetic, symbiotic, and cellular mechanisms involved in the gradual response and subsequent collapse of *Cassiopea* holobionts during acute heat stress.

To this end, we studied the symbiotic interactions and the nutritional status of the *Cassiopea* medusae in a controlled heat stress experiment. The intrinsic heat stress response of unfed *Cassiopea andromeda* holobionts (Forskål, 1775) to prolonged elevated temperatures was investigated. Physiological and elemental analyses were combined with isotope labeling and correlative scanning electron microscopy (SEM) and Nanoscale Secondary Ion Mass Spectrometry (NanoSIMS) imaging to study the impact of heat stress on the metabolism of the symbiotic partners. This approach permitted the identification of similarities with well-described heat stress responses of other photosymbiotic cnidarians such as corals and sea

anemones. It also revealed some of the distinct characteristics that potentially explain the high heat tolerance of the *Cassiopea* holobiont.

Materials and methods

Animal husbandry

Forty-eight *Cassiopea* medusae with bell diameters around 2 cm (1.95 ± 0.16 cm, mean $\pm$ SD) and a generally healthy appearance (intact and round bell, constant pulsation, opened oral arms) were used for this experiment. These medusae were bred and reared from strobilating polyps in our culture aquarium. This culture was established from an initial population of medusae acquired from DeJong Marinelife in the Netherlands. Genetic identification by amplification and sequencing of fragments of the COI (mitochondrial cytochrome oxidase subunit I) regions from three individuals from this culture identified the species as *Cassiopea andromeda* (data not shown). In the 200-L culture tank, the medusae were maintained in artificial seawater (ASW) prepared from sea salt (Reefs Salt, Aquaforest) at a salinity of 35 ppt and $25.3 \, ^\circ\text{C} \pm 0.2 \, ^\circ\text{C}$, illuminated with approximately 100 µmol photons m^{-2} s^{-1} from LED lights on a 12 h:12 h day:night cycle. Before the experiment, the animals were fed ad libitum two to three times a week with freshly hatched *Artemia salina* nauplii.

Design of the thermal stress experiment

Three days before the beginning of the experiment, the selected medusae were transferred to the experimental setup for acclimatization.

The experimental setup consisted of two identical units, one for each condition, (i.e., control and heat stress), each including a main 15-L water bath, a circulation pump and a heater to maintain a homogeneous temperature (Figure S1). The water baths were closed by a transparent PVC cap to avoid evaporation and salinity fluctuations. Inside each water bath, six independent 500-mL transparent experimental acrylic containers were equipped with transparent lids and had constant air bubbling to maintain well-oxygenated conditions (Loft food container, Rotho, Switzerland). Each container was filled with 400 mL of ASW, had no water exchange with the main water bath, and held four medusae. Animals were kept on a 12 h:12 h day:night cycle with LED lights (VIPARSPECTRA V165, USA) providing approximately 110 µmol photons m^{-2} s^{-1}. Each day, the salinity in the experimental containers was measured and 90% of the ASW was replaced with fresh ASW at the same temperatures as the thermal baths. Both light and salinity in the experimental units were maintained at levels similar to the animal culture conditions to avoid the confounding factors of osmotic and light stress. During the acclimatization and experimental period (a total of 13 days), animals were not fed to exclude potential confounding effects of heterotrophic nutrient acquisition.

The temperature in both water baths was constantly recorded using a submersible temperature logger (Pendant Temperature/Light 64 K Data Logger, HOBO, US) placed in a separate acrylic container filled with 400 mL of ASW without medusae. For both experimental conditions, units were maintained at a temperature of approximately 27 °C (control: 27.3 ± 0.5 °C, heat stress: 27.0 ± 0.8 °C) during an acclimatization period of 2 days. At the beginning of the experiment (day 1), the temperature of the heat stress condition was gradually ramped up to a final temperature of about 34 °C, which was reached on day 5 and subsequently maintained at 34.1 ± 0.5 °C throughout the experiments, i.e., for 7 days (Fig. 1A). The final temperature of 34 °C was chosen for the heat stress condition because previous studies documented bleaching and holobiont collapse at this temperature in *Cassiopea* [46, 48]. The control animals remained at an average temperature of 27.2 ± 0.6 °C throughout the experiment.

To assess the impact of temperature on medusae physiology throughout the experiment, daily measurements of pulsation rate, maximum quantum yield, and bell diameter were carried out at the end of the dark period (Fig. 1). Isotopic labeling, incubations, and sampling of water and twelve medusae from three predefined containers occurred on days 5 (SP1) and 11 (SP2), corresponding to the 1st and the 7th day at the final temperature (34 °C) of the heat stress exposure (Figs. 1A and S1).

Daily measurements of pulsation rate, maximum quantum yield, and bell diameter

Every morning, within 1.5 h before the light period, two sets of measurements on dark-acclimated medusae were performed using low-intensity red light to not affect their symbiotic photophysiology. First, the night pulsation rates were assessed by counting the bell contractions of each medusa for 1 min. Medusae presenting unsynchronized pulsations (spasms) were counted as not pulsating. Medusae presenting "melted" and disintegrated bell tissues were considered dead and removed from the experiment. Then, the dark-acclimated or maximum quantum yield (Fv/Fm) was measured by pulse-amplitude modulation (PAM) fluorometry using a MINI-PAM-II (blue version; Walz GmbH, Germany) with a 5.5-mm fiber optic targeting the center of the medusae.

Each day, at the beginning of the light cycle, each experimental container was carefully placed on a scaled board and the medusae were photographed with a fully expanded bell to record their bell diameter. For this, each experimental container was removed from the water
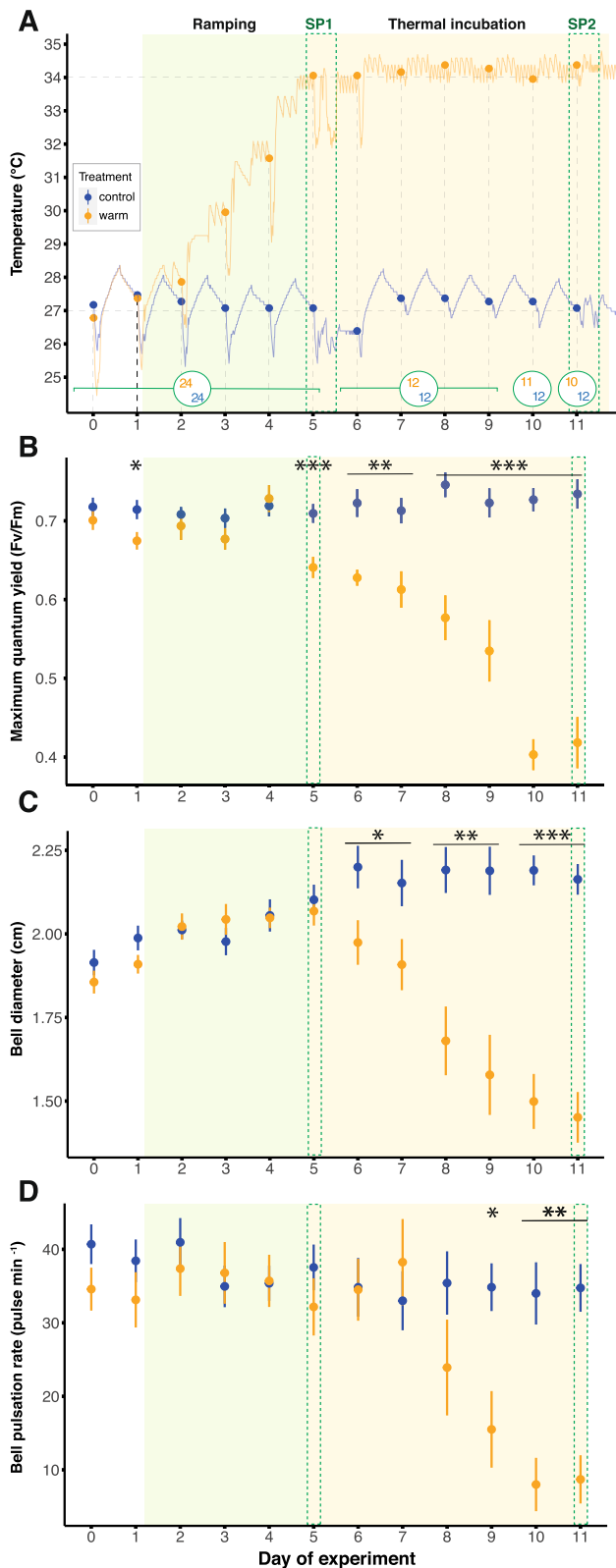
Fig. 1 Thermal treatment and daily measurements on *Cassiopea andromeda* holobionts. **A** Temperature profiles of the two thermal treatments over the course of the experiment. The filled circles indicate the seawater temperature at the start of daily measurements. Numbers inside the larger open circles indicate the number of animals for each treatment at the corresponding time. **B** Maximum quantum yield (Fv/Fm) of the algal symbionts. **C** Evolution of bell diameters and **D** bell pulsation rates of the medusae over time. Filled circles and error bars indicate mean ± SE for control (blue) and heat stress (orange) treatment respectively. Asterisks indicate significant differences between treatments for respective time points (*$p < 0.050$, **$p < 0.010$, ***$p < 0.001$). SP = sampling point

baths for less than 2 min to avoid excessive cooling of the contained water, followed by water exchange.

Physiological parameters

On each of the two sampling points (SP1 and SP2), six medusae (two medusae randomly selected from three predefined containers each, Figure S1) per condition were sampled for physiological measurements, except for the heat-stressed condition at SP2 (only four medusae were sampled due to early mortality).

To assess the ammonium (NH_4^+) uptake and release by the medusae, they were transferred individually into glass beakers containing 40 mL of freshly prepared ASW prewarmed to the respective treatment temperatures and placed inside the corresponding water baths. Additionally, one beaker containing only seawater (no medusae) was placed in each water bath to assess and correct for the potential evolution in NH_4^+ concentration in seawater unrelated to the medusa's presence. After 6 h of incubation in the light, the ASW from each beaker was collected and replaced with temperature-matched seawater. The collected water samples were filtered through 0.22-µm PES filters (pre-rinsed with Milli-Q water and an aliquot of sample water, which was discarded), and NH_4^+ concentrations were immediately measured using a Smartchem450 wet chemistry analyzer (AMS Alliance, Italy).

Following water sampling, the six medusae were collected to assess their wet weight, host protein content, Symbiodiniaceae density, and chlorophyll *a* content. Excess water was removed, and medusae were placed in a pre-weighted 5-mL round-bottom culture tube and weighed using a precision balance. Cold 2×PBS was added by taking into account the wet weight of the medusa and aiming for a final volume of 3 mL (the volume of PBS added was 3 mL minus the medusae volume, estimated from the medusae weight and assuming a density of 1 g mL^{-1}). The medusae were then homogenized on ice in 2×PBS using a Polytron Immersion Dispenser (Kinematica, Malters, Switzerland) for at least 30 s until

the tissue slurry was visibly homogeneous. To separate the host fraction from the Symbiodiniaceae, two equal aliquots of 1.3 mL of the tissue homogenate were transferred into Eppendorf tubes and centrifuged at $3000 \times g$

$$\text{Chlorophyll } a\left(\mu g \, mL^{-1}\right) = 11.43*(OD(664)-OD(750))-0.64*(OD(630)-OD(750))$$

and 4 °C for 3 min. The supernatants containing the host fraction were transferred into a 2-mL cryogenic tube, snap frozen in liquid nitrogen, and stored at −80 °C until further processing of host protein content measurements. The pellets containing the Symbiodiniaceae were resuspended in 1 mL of 2×PBS, transferred into a 2-mL cryogenic tube, snap frozen, and stored at −80 °C for subsequent Symbiodiniaceae and chlorophyll *a* quantification.

The host protein content of medusae was assessed in three technical replicates, using a Pierce Rapid Gold BCA Protein Assay Kit (Thermo Fisher Scientific, Germany), following the manufacturer's instructions for the standard microplate protocol. The host fraction of the tissue homogenate was gently thawed on ice. Technical triplicates of each sample were transferred into a flat-bottom 96-well plate. Protein content was assessed in a BioTek Synergy H1 high sensitivity plate reader (BioTek Instruments, USA) by measuring the absorbance at 480 nm and calibrated against absorbances of a serial dilution of bovine serum albumin (BSA) protein standard (range of standard curve from 0 to 2 μg mL^{-1}), which were assayed alongside the medusa samples.

To assess the density of Symbiodiniaceae, the algal symbiont pellet was gently thawed on ice and resuspended by vigorous vortexing, and four technical aliquots of 10 μl were analyzed using a CellDrop™ automated Cell Counter (DeNovix, USA). Automated cell count measurements were based on cell size and chlorophyll autofluorescence in the red channel. Finally, averaged Symbiodiniaceae counts for each medusa were standardized by host protein as a proxy of host biomass.

The chlorophyll *a* content was quantified from an aliquot of 700 μl of the Symbiodiniaceae fraction (the same aliquot from which Symbiodiniaceae cells were counted). Symbiodiniaceae cells were first rinsed by two centrifugation steps (3000×*g* at 4 °C for 3 and 5 min) with resuspension of the pellet in 1 mL of 2×PBS in between. The pellets were then resuspended in 500 μl of ice-cold ethanol (95%) and incubated in the dark at 4 °C under constant rotation overnight (14 h) for chlorophyll extraction. Finally, 200 μl of each sample in duplicate was transferred into a flat-bottom 96-well plate, along with duplicates of the solvent for the blank standardization. The absorbance of each sample was measured at 630, 664, and 750 nm

with a BioTek Synergy H1 high sensitivity plate reader (BioTek Instruments, USA), and the chlorophyll *a* content was calculated as follows (with turbidity correction, Jeffrey and Humphrey,1975):

Chlorophyll *a* content was then standardized to the host protein content of each individual medusa.

Elemental composition
To measure the impact of temperature on the total organic carbon and nitrogen content of the medusa, three individuals per treatment and sampling point were sampled. After seawater was carefully removed, the medusae were weighed in a pre-weighed 5 mL round-bottom culture tube, and a volume of 2×PBS was added to a final volume of 3 mL, as described above. The tissue was then homogenized, aliquoted, and the host and dinoflagellate fractions were separated and snap frozen with an additional rinsing step for the Symbiodiniaceae prior to snap freezing in liquid nitrogen (3000×*g* at 4 °C for 3 min, and resuspension of the pellet in 1 mL of 2×PBS). Frozen host and Symbiodiniaceae fractions were freeze-dried for 2 days. Approximately 2.5 ± 0.4 and 10.5 ± 1.5 mg of the respective dried sample fractions were then weighed in duplicate for each sample and encapsulated in aluminum for carbon and nitrogen analysis respectively. The elemental analysis/isotope ratio mass spectrometry (EA/IRMS) was performed using a Carlo Erba 1108 (Fisons Instruments, Italy) elemental analyzer connected via a ConFlo III split interface to a Delta V Plus isotope ratio mass spectrometer (Thermo Fisher Scientific, Germany) operated under continuous helium flow [54]. The carbon and nitrogen contents (in wt. %) were determined from the EA/IRMS peak areas and converted into the atomic abundance to calculate atomic C:N ratios for each sample.

Stable isotope labeling experiment for nutrient tracking and histological analyses
In order to investigate the impact of the temperature on the uptake and exchange of nutrients between the medusae and the Symbiodiniaceae, three medusae were incubated in isotopically labeled ASW for each condition and sampling point.

One day before labeling and sampling, ASW was freshly prepared with Milli-Q water, depleted of dissolved organic carbon by acidification with HCl (4 M) to a pH < 3, and maintained under constant bubbling with air for at least 4 h. This ASW was then supplemented with ^{13}C-bicarbonate (Sigma 372382) to a final concentration of 3 mM, and the pH of the solution increased again to

8.1 with 1 M NaOH solution. Finally, ^{15}N-ammonium chloride (Sigma 299251) was added to a final concentration of 3 μM. After thorough mixing, the labeled ASW was split into two aliquots and thermally equilibrated overnight at the temperatures for the control and heat stress treatments, respectively.

Incubation with isotopically labeled bicarbonate and ammonium was initiated at the beginning of the light period by placing three medusae into glass beakers filled with 40 mL of thermally equilibrated and isotopically labeled ASW medium for 6 h. After 3 h into this incubation, 30 mL of isotopically labeled ASW medium was replaced to ensure constant concentrations of ^{13}C-bicarbonate and ^{15}N-ammonium, respectively. At the end of the incubation, the medusae were sampled and cut into quarters using clean razor blades. Two of these quarters were fixed immediately for correlative SEM and NanoSIMS imaging (4% paraformaldehyde, 2.5% glutaraldehyde in 0.1 M Sorensen's buffer, 9% sucrose), and one quarter was fixed for paraffin embedding and light microscopy (4% paraformaldehyde in 0.1 M Sorensen's phosphate buffer, 9% sucrose). Fixed samples were maintained at 4 °C until further processing. To have an unlabeled control sample, one medusa within the same size range was sampled directly from the culture tank, dissected, preserved, and processed in the same manner.

Nutrient assimilation and cellular ultrastructure by correlative SEM and NanoSIMS imaging

The bell tissue samples fixed for resin embedding (for correlative SEM and NanoSIMS imaging) were processed after at least one night of fixation at 4 °C. First, the samples were rinsed with Sorensen's buffer (0.1 M) to remove the fixative and dissected to obtain a small piece of tissue (around 4 mm^3) from the center of the bell. To preserve the lipid fraction of the samples, the small tissue pieces were post-fixed for 1 h with osmium tetroxide (OsO$_4$ 1%, 1.5% potassium hexacyanoferrate II in 0.1 M Sorensen phosphate buffer) under constant agitation and rinsed twice in Milli-Q water for 20 min. Using a tissue processor, the samples were then subjected to a serial dehydration in ethanol (30, 70, and 100% ethanol in Milli-Q water), to facilitate a progressive Spurr resin infiltration (30, 70, and 100% Spurr resin in absolute ethanol). Once infiltrated, the samples were placed into molds filled with 100% Spurr resin and cured at 60 °C for 48 h. Thin sections (200 nm) were cut from the resin blocks using an Ultracut S microtome (Leica Microsystems) and a diamond knife (DiATOME) and collected on clean silicon wafers.

In order to add contrast and to visualize the subcellular structures present in the tissues, sample sections were post-stained with 1% uranyl acetate and Reynolds Lead Citrate before imaging by scanning electron microscopy (SEM, GeminiSEM 500, Zeiss; 3 kV, aperture size of 30 μm, and a working distance of 2.9 to 2.3 mm) with an energy selective backscatter detector (EsB, grid of 130 V; Zeiss).

To image the distribution of isotopic enrichments within subcellular structures visualized in SEM images, the same sections were sputter coated with a 12-nm gold layer (using a Leica EM SCD050 gold coater) and transferred to a Nano Secondary Ion Mass Spectrometry (NanoSIMS) 50 L for analysis [55]. In the NanoSIMS, the pre-sputtered samples were bombarded with a Cs$^+$ primary ion beam at 16 keV with a current of around 2 pA, focused to a spot size of ca. 150 nm. This beam was rastered over an area of 45×45 μm with a dwelling time of 5000 μs per pixel. The secondary ions $^{12}C_2^-$, $^{13}C^{12}C^-$, $^{14}N^{12}C^-$, $^{15}N^{12}C^-$ were counted individually in electron multiplier detectors at a mass resolution power of around 9000 (Cameca definition), which resolves potential interferences in the mass spectrum. From the resulting isotope maps (45×45 μm, 256×256 pixels, superposition of 6 drift-corrected images), regions of interest (ROIs) were drawn around the different tissue compartments, i.e., Symbiodiniaceae, amoebocytes (excluding the Symbiodiniaceae), and the epidermis. For each ROI, the isotopic ratio enrichments established through the ratios $^{13}C^{12}C^-/^{12}C_2^-$ and $^{15}N^{12}C^-/^{14}N^{12}C^-$ were quantified against a control sample with natural isotopic compositions prepared and analyzed in an identical manner, using the NanoSIMS software L'Image (v.10–15-2021, developed by Dr. Larry Nittler). Isotope enrichments are reported in the delta (δ) notation as followed:

$$\delta^{13}C(\text{‰}) = \left(\frac{rC(sample)}{rC(unlabeled)} - 1 \right) \times 1000$$

and

$$\delta^{15}N(\text{‰}) = \left(\frac{rN(sample)}{rN(unlabeled)} - 1 \right) \times 1000$$

where rC$_{(sample)}$ and rC$_{(unlabeled)}$ are the count ratios of $^{13}C^{12}C^-/^{12}C_2^-$ in the sample and in an unlabeled control, respectively. rN$_{(sample)}$ and rN$_{(unlabeled)}$ are the count ratios of $^{15}N^{12}C^-/^{14}N^{12}C^-$ in the sample and in an unlabeled control, respectively.

Compartments were only considered to be significantly enriched if the average of the delta value of the measured ROIs were more than two standard deviations above the average delta values measured in similar compartments in an unlabeled sample. The number of images and ROIs per compartment and sample is reported in the supplementary information (Table S1).

To estimate the symbiont contribution to host metabolism, the mean of ratios of ^{13}C enrichments in host amoebocytes and their algal symbionts was calculated: each ^{13}C enrichment value of an amoebocyte was divided by the mean of the ^{13}C enrichments of the symbionts hosted within this amoebocyte. Only viable amoebocytes and symbiont cells that were significantly enriched were included in this calculation.

Histological characterization of the tissue structure and cell density in the medusae bell tissue by light microscopy

The bell tissue fixed for paraffin embedding underwent serial dehydration in ethanol, then xylene before infiltration and embedding in paraffin. Sections 4 μm thick of paraffin-embedded samples were cut and placed on a glass slide, dewaxed, and stained with hematoxylin and eosin (H&E) before being imaged by transmitted light microscopy with a Keyence VHX-7000 digital microscope. For each sample, three images containing the oral epidermis, gastric cavity, and surrounding mesoglea were taken at identical magnification and settings. Two different regions of the mesoglea were assessed on the images: the oral mesoglea, located between the oral epidermis and the gastrodermis and hosting most of the dinoflagellates, and the inner mesoglea, located below the gastrodermal tissue layers and hosting fewer dinoflagellates. The area of the entire oral and inner mesoglea present in each image was assessed manually using ImageJ (ImageJ2, version: 2.920/1.53t). The number of algal symbiotic cells and host nuclei in each region were manually counted and normalized by the corresponding mesoglea area in each image to obtain symbiotic cell or host nuclei density.

Statistical analysis

All analyses were performed in R (version 4.2.0, [56]). All response parameters were measured daily among treatments and were analyzed for each experimental day using ANOVA (for normally distributed data, considered true when $p < 0.05$ for Shapiro–Wilk test) or Kruskal–Wallis (when the normal distribution assumption of data was violated), followed by multiple comparison corrections of p-values based on false discovery rate (FDR).

For the physiological measurements and the ratio of ^{13}C enrichment between host amoebocytes and their algal symbionts, the influence of the treatment and sampling point on the data were analyzed using a two-factorial ANOVA (normal distribution of the data as confirmed by Shapiro–Wilk test, $p > 0.05$) followed by Tukey's honestly significant differences (HSD) post hoc comparison. In the cases where ANOVA results indicated a significant interaction between treatments and sampling points but

Tukey's HSD did not allow resolving treatment effects for individual sampling points, one-factorial ANOVA was used for individual sampling points (indicated in the figures with asterisks in brackets). The ammonium uptake data were square root transformed following the addition of a constant to avoid negative values before analysis to assure the homogeneity of the variances required for the ANOVA. The isotopic enrichment across treatments and sampling points was analyzed with a linear mixed model (LMM) introducing the three biological replicates as a random variable. This was followed by Tukey's HSD post hoc comparison. In the cases where LMM results indicated a significant interaction between treatments and sampling points but Tukey's HSD did not resolve treatment effects for individual sampling point, one-factorial ANOVA or Kruskal–Wallis was used for individual sampling point (indicated in the figures with asterisks in brackets).

Finally, differences in cell or nuclei density in the mesoglea among treatments for sampling point 2 were analyzed with a LMM, using the three biological replicates as a random variable. All data in the text are presented as mean ± SD unless stated otherwise.

Results

Response of *Cassiopea andromeda* to elevated seawater temperature

During the ramping period of the experiment (Fig. 1A), the increase in seawater temperature had no detectable effect on the physiology of the medusae (Fig. 1B–D). However, once the maximum temperature (34 °C) was reached on day 5, the *Cassiopea* holobionts started to show the first response to heat stress compared to the control specimens. While the maximum quantum yield (Fv/Fm) of algal symbionts remained stable over time under control conditions, their heat-stressed counterparts showed a significant decline starting from day 5 of the experiment (ANOVA, $F = 14.61$, FDR-adjusted $p < 0.001$; Fig. 1B). This decline became increasingly pronounced over time, leading to a 43% reduction under heat stress (Fv/Fm = 0.42 ± 0.10) compared to control (Fv/Fm = 0.73 ± 0.06) condition on the last day of the experiment (ANOVA, $F = 77.19$, FDR-adjusted $p < 0.001$).

In addition to the photophysiological response of algal symbionts, host metrics were visibly affected by the heat stress treatment. While the bell diameters of medusae tended to increase similarly in both treatments during the ramping period, the bell diameters of heat-stressed medusae exhibited a significant decrease beginning on day 6 (ANOVA, $F = 5.98$, FDR-adjusted $p = 0.046$; Fig. 1C), resulting in an average 33% decline compared to control medusae by the end of the experiment. Likewise, the pulsation rate in heat-stressed medusae decreased
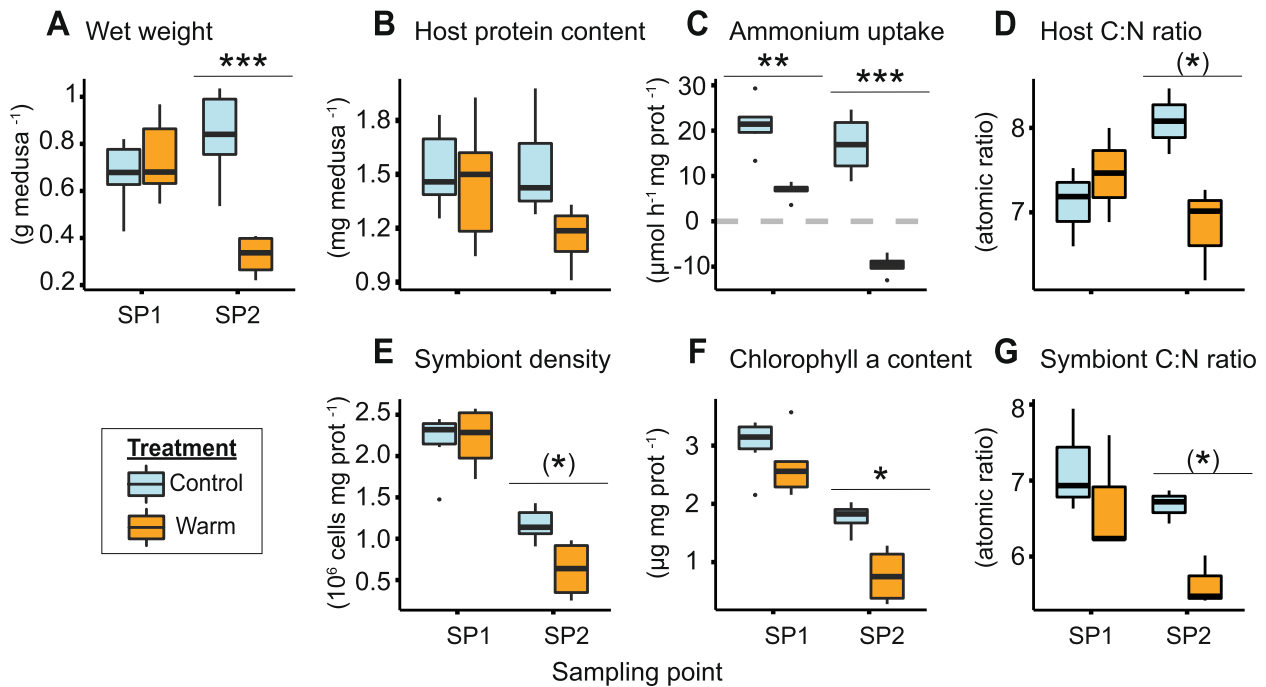
Fig. 2 Physiology and nutritional status of *Cassiopea* holobionts exposed to heat stress. **A** Medusae wet weight. **B** Host protein content. **C** Holobiont net ammonium uptake rate. **D** Host atomic C:N ratio. **E** Symbiont density per host protein, **F** Chlorophyll a content per host protein. **G** Symbiont atomic C:N ratio. Sampling points correspond to days 5 (SP1) and 11 (SP2) of the experiment. Individual groups were compared using Tukey's HSD (indicated above the boxplots). Asterisks indicate significant differences between treatments (*$p < 0.050$, **$p < 0.010$, ***$p < 0.001$). Asterisks in brackets show significant differences when only SP2 is considered. Number of biological replicates per condition: **A**, **B**, **C**, **E**, **F** $n = 6$ except for SP2 under heat stress where $n = 4$; **D**, **G** $n = 3$

significantly from day 9 onwards (ANOVA, $F = 10.28$, FDR-adjusted $p = 0.016$) with a 75% decline by the end of the experiment (Fig. 1D). This decrease in pulsation rate in heat-stressed medusae was also associated with spasms and/or total immobility in some individuals.

Ultimately, the first cases of mortality were observed in heat-stressed medusae towards the end of the experiment, beginning on day 10 (Fig. 1A).

Heat stress alters the physiology and the nutritional status of *Cassiopea andromeda*

The *Cassiopea* host exhibited a clear physiological response to heat stress already a few days after reaching 34 °C (i.e., around days 6 and 7 of the experiment; Fig. 1) and this trend continued until the end of the experiment, resulting in several pronounced differences between the two sampling points SP1 (day 5) and SP2 (day 11) (Fig. 2).

The wet weight of the medusae was unchanged at SP1 (Tukey's HSD, $p = 0.891$), but showed a significant 61% decrease at SP2 under heat stress (Tukey's HSD, $p < 0.001$; Fig. 2A). The host protein content per medusa exhibited no significant effect of heat stress at SP1, but a 25% reduction (albeit not significant) at SP2 (ANOVA, $F = 2.87$, $p = 0.107$; Fig. 2B). Net ammonium uptake rates

were decreased significantly by 51% under heat stress already at SP1 (Tukey's HSD, $p = 0.009$). They even showed a negative rate (i.e., a net release of ammonium into the surrounding seawater) at the end of the experiment (Tukey's HSD, $p < 0.001$, Fig. 2C). The C:N ratios of heat-stressed host medusae remained stable at SP1 (Tukey's HSD, $p = 0.828$), but exhibited a significant 16% decrease at SP2 compared to control animals of the same time point (Tukey's HSD, $p = 0.059$). The average host C:N ratio of the control animals showed a non-significant 14% increase over the course of the experiment (Tukey's HSD, $p = 0.154$, Fig. 2D).

Despite these changes in host physiology, heat-stressed medusae showed no visual signs of bleaching, and no loss of pigmentation was observed during the experiment (Figure S2). Nonetheless, the physiology and elemental compositions of the symbionts were clearly affected by heat stress at both sampling points (Fig. 2E–G). The density of symbiont cells relative to host protein content in heat-stressed animals decreased significantly by 46% at SP2 (ANOVA considering only SP2, $F = 9.54$ $p = 0.015$; Fig. 2E). The chlorophyll *a* content of symbionts (per mg of host protein) became significantly reduced during heat stress (ANOVA, $F = 7.29$, $p = 0.015$) with a 55%

decline compared to control conditions at SP2 (Tukey's HSD, $p = 0.011$, Fig. 2F) and the symbiont C:N ratio was significantly reduced during heat stress, down by 16% at SP2 (ANOVA, $F = 5.55$, $p = 0.046$) compared to control conditions (ANOVA considering only SP2, $F = 20.66$, $p = 0.011$, Fig. 2G). However, when normalized to medusa wet weight, neither symbiont densities nor chlorophyll *a* content was significantly affected by heat stress (symbiont densities per wet weight: LMM, $F = 0.02$; $p = 0.894$; chlorophyll *a* per wet weight: LMM, $F = 0.45$, $p = 0.513$; Figure S3).

Heat stress reduces nutrient assimilation in the symbiosis
Overall, NanoSIMS analyses revealed that heat stress had pronounced effects on ^{13}C-bicarbonate and ^{15}N-ammonium assimilation by the symbiotic partners (Fig. 3).

Compared with the control condition, heat stress caused a significant reduction in ^{13}C enrichment in algal symbionts (LMM, $X^2 = 64.54$, $p < 0.001$, Fig. 3A), in the host amoebocyte cells containing them (LMM, $X^2 = 24.86$, $p < 0.001$, Fig. 3B), and in the host epidermis (LMM, $X^2 = 7.30$, $p = 0.006$, Figure S4A). In more detail, at SP1, the ^{13}C enrichment of amoebocytes was insignificantly lower in heat-stressed animals (Tukey's HSD, $p = 0.189$), while ^{13}C enrichment of algal symbionts remained relatively stable (Tukey's HSD, $p = 0.115$). At SP2, ^{13}C enrichment of both amoebocytes and symbionts under heat stress declined by 94 and 82%, respectively (Host: Tukey's HSD, $p = 0.006$; symbiont: Tukey's HSD, $p < 0.001$; Fig. 3A,B). Furthermore, the average of the ratios of ^{13}C enrichments in amoebocytes and their algal symbionts (excluding algae-amoebocyte pairs without significant enrichment) was reduced by 60% (ANOVA, $F = 6.57$, $p = 0.013$) compared to control conditions (Tukey's HSD, $p = 0.012$, Fig. 3C).

These quantitative changes in ^{13}C enrichment were accompanied by marked differences in the subcellular spatial distribution within the tissues of heat-stressed medusae at SP2 (Fig. 3F,G,I,J). In the host tissue of control animals, strong ^{13}C enrichments were concentrated in hot spots corresponding to lipid droplets (dark structures stained by osmium in SEM images, Fig. 3F,G). During heat stress, however, these lipid droplets appeared less abundant in the epidermis and almost absent in the amoebocytes, and thereby likely contributing to a lower ^{13}C enrichment in the host (Fig. 3I,J).

In the symbionts, ^{13}C enrichments were primarily located around the pyrenoid and lipid droplets under control conditions (Fig. 3G). Under heat stress, however, ^{13}C enrichment hotspots were overall less pronounced in symbiont cells (Fig. 3J) with some cells exhibiting almost no detectable ^{13}C enrichment.

While heat stress also affected ^{15}N-ammonium assimilation by the symbiotic partners, the extent was less pronounced. Heat stress caused no overall significant effect on ^{15}N-ammonium assimilation across sampling points in the host epidermis (LMM, $X^2 = 0.37$, $p = 0.541$, Figure S4B), the amoebocyte cells (LMM, $X^2 = 2.07$, $p = 0.150$, Fig. 3E), and the algal symbionts they contained (LMM, $X^2 = 2.57$, $p = 0.109$, Fig. 3D). Furthermore, the interaction of the sampling time and heat stress factors had no significant effect on the reduction of ^{15}N enrichment of the host epidermis (LMM, $X^2 = 0.41$, $p = 0.521$), but had an impact on the amoebocytes (LMM, $X^2 = 5.77$, $p = 0.016$) and algal symbionts (LMM, $X^2 = 5.12$, $p = 0.024$). When analyzed per time point, the ^{15}N enrichment in the amoebocytes and symbionts of heat-stressed medusae remained stable compared to the control treatment at SP1 (Amoebocyte: Kruskal–Wallis at SP1, $X^2 = 1.85$, $p = 0.172$; symbiont: Kruskal–Wallis at SP1, $X^2 = 2.43$, $p = 0.119$). At SP2, however, significant decreases (60% and 84%, respectively) were observed for amoebocytes (-60%, Kruskal–Wallis at SP2, $X^2 = 23.86$, $p < 0.001$) and algal symbionts (-84%, Kruskal–Wallis at SP2, $X^2 = 87.09$, $p < 0.001$). This was accompanied by differences in the subcellular spatial distribution of ^{15}N-ammonium enrichment between temperature treatments at SP2 (Fig. 3F,H,I,K). Specifically, ^{15}N-ammonium enrichment was largely homogenous in the host tissues, with strong enrichment in the symbionts under control conditions

(See figure on next page.)
Fig. 3 Temperature effects on enrichment and (sub)cellular localization of isotopically labeled carbon and nitrogen in heat-stressed medusae. **A** ^{13}C enrichment from ^{13}C-bicarbonate (H^{13}CO$_3^-$) assimilated into algal symbiont cells and **B** translocated to their host amoebocyte cells. **C** Ratio of ^{13}C enrichment between host amoebocytes and their algal symbionts. **D** ^{15}N-enrichment induced by the assimilation of ^{15}N-ammonium (NH$_4^+$) into algal symbiont cells and **E** into host amoebocytes. Sampling points correspond to days 5 (SP1) and 11 (SP2) of the experiment. Individual groups were compared using Tukey's HSD (indicated above the boxplots). Asterisks indicate significant differences between treatments (*$p < 0.050$, **$p < 0.010$, ***$p < 0.001$). Asterisks in brackets show significant differences when only SP2 is considered. **F–K** Correlative SEM (**F**, **I**) and NanoSIMS (**G**, **H**, **J**, **K**) isotope ratio images of medusa sections under control conditions (**F–H**) and heat stress (**I–K**) at SP2. The corresponding ^{12}C$_2^-$ and ^{14}N^{12}C$^-$ images are available in Figure S5. The SEM images are artificially colored, with oral epidermis (oral epi) in beige, mesoglea (m) in blue, amoebocyte (am) in yellow, amoebocytes nuclei in purple, symbionts (s) in green, and lipid droplets (ld). The color scales of the NanoSIMS images are logarithmic
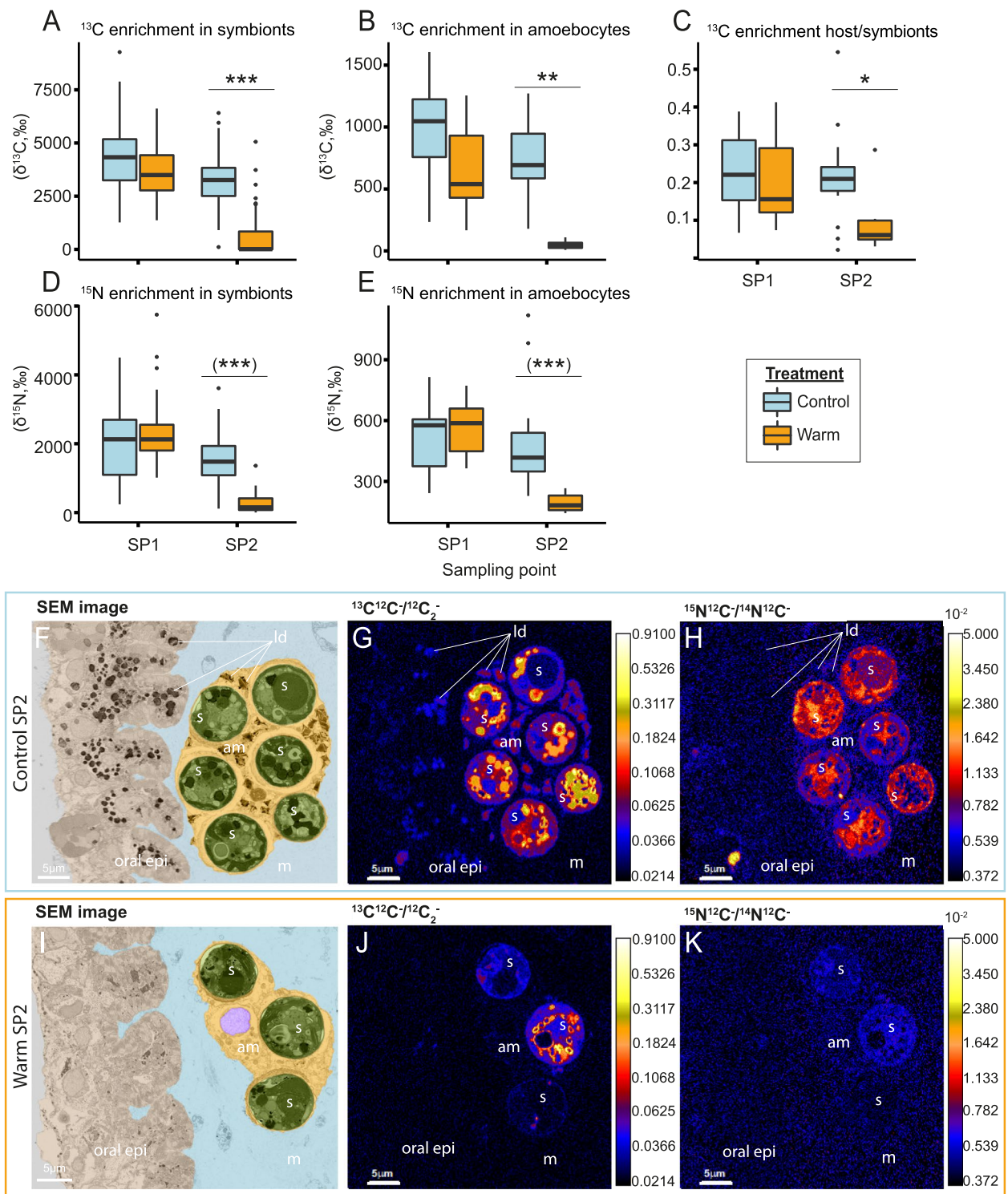
Fig. 3 (See legend on previous page.)

(Fig. 3F,H). During heat stress, however, ^{15}N enrichment was less pronounced in the host tissue and substantially reduced in the symbionts, with some cells showing no discernible enrichment (Fig. 3I,K).

Impact of temperature on tissue and cells ultrastructure

Light and electron microscopy of the bell tissues revealed an increase in the density of host cells in the mesoglea in heat-stressed medusae at SP2. This was most pronounced

in the oral mesoglea and was accompanied by substantial in hospite degradation of algae cells (Fig. 4, S6).

Light microscopy revealed a pronounced increase in the density of host nuclei in the mesoglea during heat stress (LMM, $X^2 = 13.63$, $p < 0.001$, Fig. 4A–D). Interestingly, this increase was more pronounced in the oral compared to the inner mesoglea (6- and threefold increase, respectively; LMM, $X^2 = 37.09$, $p < 0.001$, Fig. 4G). The density of algal symbionts in the oral mesoglea remained unchanged by the heat treatment (LMM, $X^2 = 1.04$, $p = 0.308$). The symbiont density in the inner mesoglea increased slightly, potentially due to the migration of symbiotic amoebocytes towards the gastric cavity for symbiont expulsion (LMM, $X^2 = 3.88$, $p = 0.049$).

SEM imaging corroborated the observation made by light microscopy. While host nuclei in the oral mesoglea of control animals were evenly distributed, host nuclei of heat-stressed animals appeared in clusters indicating an aggregation of amoebocyte cells (Fig. 4E,F). Importantly, the symbiotic algae in these amoebocyte clusters displayed clear signs of stress with different degrees of deterioration during heat stress. Specifically, these symptoms included disorganization of cellular contents and thylakoids and pronounced internal degradation of cell contents (Fig. 4H).

Discussion

Climate change has resulted in an unprecedented decline of tropical coral reef ecosystems at a global scale due to the demise of their main ecosystem engineers, reef-building corals. In corals, this decline is partly linked to the breakdown of symbiotic nutrient cycling, leading to host starvation that ultimately results in coral bleaching and mortality [8, 26, 57]. In contrast, the upside-down jellyfish *Cassiopea* is projected to thrive under the current and future conditions despite hosting similar photosynthetic symbionts [53]. Here, we were able to show that severe heat stress enhanced host catabolism and reduced the contribution of algal symbionts to the metabolism of *Cassiopea*, creating a state of host starvation. While this stress response resembles that observed in corals, our data suggest that some mechanistic aspects of the breakdown of the symbiosis reflect the unique properties of the *Cassiopea* holobiont. Specifically, a high occurrence of in hospite degradation of algal symbionts inside the amoebocytes coupled with animal shrinkage (i.e., a reduction in body size and wet weight) led to a delayed and "invisible" bleaching response.

Heat-induced host catabolism and carbon starvation

In this study, severe heat stress caused host energy limitation and the metabolic switch towards catabolism, leading to a significant depletion of carbon reserves and a visible shrinkage of *Cassiopea* medusae.

We observed a pronounced reduction of C:N ratios in heat-stressed *Cassiopea* (Fig. 2D) coupled with a reduction of lipid droplets within the amoebocytes (Figs. 3G,J, 4E,F and S6) and a less pronounced decrease in protein content (Fig. 2B). Together, these responses point to an enhanced consumption and depletion of carbon reserves in the host metabolism. The metabolic activity of ectothermic animals tends to increase with temperature [58]. Acute heat stress thus stimulates the respiratory energy demand of Cnidaria, including scyphozoan medusae [52, 59, 60]. Our results suggest that *Cassiopea* consumed its energy reserves in response to such a heat-induced increase in energy demand. This is consistent with a previous study documenting the consumption of carbon reserves, more specifically of glucose and glycogen reserves by the aposymbiotic scyphozoan medusa *Stomolophus meleagris* during heat stress [59].

In addition to enhanced consumption of sugar and lipid reserves, the progressive metabolic switch from anabolism to catabolism under heat stress was also directly reflected in the nitrogen metabolism of the holobiont. The measured decrease in net ammonium assimilation at SP1 and the net release of ammonium at SP2 (Fig. 2C) coupled with a (non-significant) decrease in host protein content (Fig. 2B) indicate that the host gradually shifted towards a catabolic degradation of protein reserves during heat stress. In an anabolic state, cnidarian hosts utilize carbon backbones for amino acid synthesis by assimilating ammonium. In a catabolic state, proteins and amino acids are used as a carbon source for energy metabolism resulting in the production of excess ammonium by the host [26, 61]. Our findings suggest that the

(See figure on next page.)

Fig. 4 Temperature effects on the ultrastructure and cell density of the bell tissue of *Cassiopea andromeda* medusae. **A–D** Light microscopy images and **E**, **F**, **H** SEM images of the medusae in control (**A**, **C**, **E**, i.e., left column) and heat stress conditions (**B**, **D**, **F**, **H**, i.e., right column). **E** and **F** are artificially colored for better visualization with oral epidermis and gastrodermis in beige, mesoglea in blue, amoebocyte(s) in yellow, amoebocyte nuclei in purple, and symbionts in green. **G** Impact of heat stress on the density of symbiont cells and host nuclei in the oral (delineated by green dotted line) and inner mesoglea (delineated by red dashed line) illustrated in **C** and **D**. Asterisks indicate significant differences between treatments (*$p < 0.050$, **$p < 0.010$, ***$p < 0.001$). **H** SEM image exhibiting the intracellular degradation (white arrowhead) and disorganized thylakoids (black arrowhead) in heat-stressed symbionts. SW: seawater, oral epi: oral epidermis, m: mesoglea, am: amoebocyte(s), n: amoebocytes nuclei, s: symbionts, gast: gastrodermis, gc: gastric cavity)
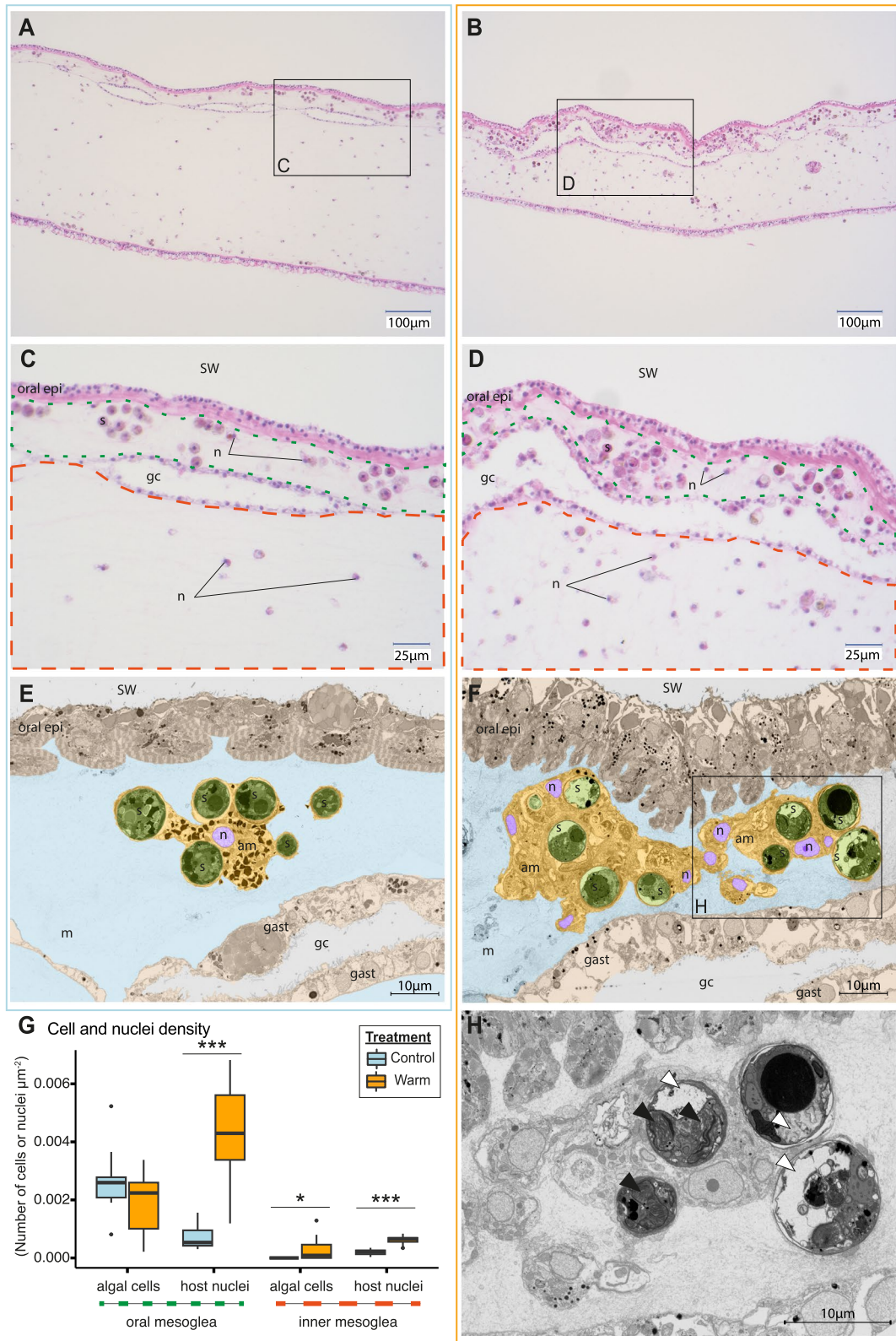
Fig. 4 (See legend on previous page.)

increased energy requirements during heat stress may have resulted in the gradual consumption of glycogen and lipid reserves and, eventually, a breakdown of proteins in the host.

Importantly, this catabolic consumption of host biomass was directly reflected in the phenotype and behavior of the animals during heat stress. Specifically, the observed reductions in bell diameter (Fig. 1C) and wet weight (Fig. 2A) align with previous reports documenting reductions in medusae size and weight in response to heat stress [46–48, 59]. Considering host carbon starvation during heat stress, we propose that this shrinkage is predominantly driven by the catabolic degradation of the mucopolysaccharide and collagen matrix of the mesoglea. The loss of these structural sugars and proteins, together with their ability to retain water, likely caused water loss and consequently body shrinkage in heat-stressed medusae [62–64]. This hypothesis is corroborated by reports of similar rapid change in the water content of *Cassiopea* exposed to thermal stresses [52] and similar shrinkage of *Cassiopea* and *Aurelia aurita* ephyrae during starvation without heat stress [65, 66]. Furthermore, the observation of reduced pulsation (Fig. 1D) and the onset of host mortality (Fig. 1A) implies that our unfed *Cassiopea* animals were unable to compensate for the metabolic constraints of severe heat stress over extended periods of time, here 7 days.

Disturbance of symbiotic metabolic exchange during heat stress

In contrast to heat-stressed *Cassiopea*, the animals in the control condition (i.e., 27 °C) showed no signs of carbon limitation. Although the decrease in symbiont density and the increase in C:N ratios observed during the experiment suggest a reduction of nitrogen availability in the holobiont, these animals continued to grow over the course of the experiment and maintained a stable protein content (Figs. 1C, 2A, and S2). In this context, the increased C:N ratio (Fig. 2D) and a continuous net ammonium uptake (Fig. 2C) indicate that the release of photosynthates by the algae was sufficient to fulfill the energetic carbon requirements and to support host anabolism under control conditions. Under heat stress however, host carbon starvation and body shrinkage, together with the decline in anabolic ^{13}C assimilation observed by NanoSIMS, corroborated the notion that algae-derived organic carbon was insufficient to fulfill the energetic requirements of the medusae (Fig. 3A,B). This observed reduction in ^{13}C enrichment likely resulted from the reduced assimilation and translocation and/or enhanced catabolic consumption of metabolites during heat stress. Given that both symbiotic partners showed this trend (i.e., a reduction in ^{13}C enrichment between SP1 and SP2), we suggest that heat stress reduced the relative contribution of photosynthates to the metabolism throughout the *Cassiopea* holobiont. In addition, we observed a decrease in the ratio of ^{13}C enrichments in amoebocytes over that of their symbionts during heat stress (Fig. 3C). This shift indicates that the decline in anabolic assimilation of carbon was more pronounced for the host than its symbionts during heat stress. Specifically, algal symbionts may have proportionally assimilated a larger fraction of the total photosynthate pool in their metabolism at the detriment of translocation to their host. Similar carbon retention, promoted by a decreased production and availability of photosynthates in algal symbionts, has also been described in other symbiotic cnidarians [23, 67].

Overall, this notion of reduced carbon availability in the symbiosis during heat stress is supported by the observed patterns of ^{15}N assimilation (Fig. 3D,E). The reduction in ^{15}N assimilation by both symbiotic partners during heat stress likely reflects the combined consequences of increased catabolic production of "unlabeled" ammonium in the host metabolism and reduced availability of carbon backbones for ammonium assimilation [68].

Taken together, our results suggest that heat stress shifted the *Cassiopea* holobiont from a nitrogen-limited to a carbon-limited state. Reduced fixation of photosynthetic carbon and/or enhanced catabolic consumption of host carbon content (sugars, lipids, and amino acids) coincided with the enhanced retention of photosynthates by the algae. In addition, heat stress might not only deprive the host of the nutritional benefit of harboring algal symbionts, but likely also imposes additional energy requirements on the host to mitigate the harmful impacts of hosting stressed algae (e.g., the release of reactive oxygen species).

Heat stress thus effectively undermines the ecological benefits of harboring algal symbionts for the cnidarian host and might in fact turn the symbiosis into an additional energetic burden.

"Invisible bleaching" by in hospite symbiont degradation

In contrast to the well-described bleaching response in corals, there was no evident loss of pigmentation in heat-stressed *Cassiopea* in the present study (Figure S2). Nonetheless, a marked drop in the maximum quantum yield of algal symbionts (Fig. 1B), a decline in the density of symbiont cells and chlorophyll *a* content normalized to host protein (Fig. 2E,F), and some host mortality were observed under heat stress (Fig. 1A). Therefore, the absence of visible bleaching does not imply that symbiotic breakdown did not occur in the *Cassiopea* holobiont. Rather, the loss of algal symbionts was likely concealed by the shrinkage of heat-stressed medusae

due to host starvation and water loss, as indicated by stable algal symbiont densities and chlorophyll *a* concentrations when normalized to wet weight (Figure S3). Notably, however, bleaching events characterized by a visible decrease in pigmentation of *Cassiopea* have been described previously, during experimental heat stress at a similar final temperature and incubation time [47, 48]. Hence, the absence of visible bleaching in the present study reveals that the heat stress response of *Cassiopea* may depend on the species as well as environmental and rearing conditions, life stage, and especially the nutritional status of the medusae. The fact that the medusae were unfed during our study may have accelerated host starvation and the associated body shrinkage, thus concealing the concomitant loss of symbionts, compared to other studies. While further experiments under in situ conditions should be performed, the "invisible" bleaching phenomenon observed here might partially explain the low number of bleaching events documented for *Cassiopea* in the wild [47, 50].

In corals and most other symbiotic Cnidaria, bleaching involves a multitude of mechanisms of symbiont loss, including expulsion, in hospite degradation, and host cell detachment [69]. Among these mechanisms, previous studies suggested that symbiont expulsion is the most important pathway of symbiont loss during bleaching [70]. While the presence of symbionts in the gastrodermis suggests that algal expulsion occurred, our experiment did not allow us to assess the importance of this mechanism in heat-stressed *Cassiopea*. However, our ultrastructural observations suggest that other mechanisms strongly contributed to symbiont loss in *Cassiopea*. Specifically, the high abundance of heavily damaged algal symbiont cells in the amoebocytes (Fig. 4F,H, S6) combined with the drop in algal nutrient assimilation (Fig. 3A,D) suggests a high occurrence of in hospite degradation of symbionts [71]. Contrary to corals and sea anemones, algal symbionts in scyphozoan medusae reside in amoebocyte host cells within the mesoglea, without direct contact with the gastrovascular cavity of the animal [33, 34, 50]. It is thus plausible that this unique cellular organization limits the expulsion of the symbionts and explains the observed high occurrence of in hospite symbiont degradation in these medusae. In hospite degradation may be relatively slower than expulsion and, combined with the body shrinkage of the animal, may contribute to a delay of visible bleaching in *Cassiopea*.

An autophagic immune response of *Cassiopea* to heat stress?

The in hospite degradation of algal symbionts was accompanied by an overall increase in the density of host nuclei in the mesoglea. This increase was significantly more pronounced in the oral mesoglea, which also contained the highest density of algal symbionts (Fig. 4G). While this increase in host nuclei density in the mesoglea may be partially ascribed to host body shrinkage, light microscopy and SEM imaging showed that a high number of these nuclei in the oral mesoglea were part of amoebocyte clusters surrounding the damaged symbiont cells (Fig. 4D, F and S6). In Anthozoa, amoebocytes have previously been described as effector cells in the immune response. These cells could migrate to sites of injury or infection and phagocytose foreign, malfunctioning, and damaged cells [72–74], also in the context of heat stress [75–78]. Hence, we propose that the observed clusters of amoebocytes in the mesoglea of heat-stressed *Cassiopea* can be considered as part of an autophagic host immune response to the presence of damaged cells [79]. We hypothesize that the presence of damaged symbiont cells (and potentially the damaged amoebocytes hosting them) in the mesoglea may attract amoebocytes free of symbionts, to engulf and phagocytose the damaged cells.

At this point, the mechanisms underlying the in hospite degradation of algal symbionts clearly require further study. On the one hand, the immune response could be a direct consequence of algal symbionts damaged by heat stress (necrosis). On the other hand, enhanced production of reactive oxygen species [13, 21], reduced nutrient translocation [26], and parasitic behavior of symbionts [23] may provide cues for amoebocyte cells to degrade symbiont cells or initiate host cell apoptosis.

In the sea anemone Aiptasia and symbiotic octocorals, necrosis and apoptosis seem to co-occur in the heat stress response [80–85]. Further histological and immunological studies to evaluate amoebocyte mobility and phagocytic activity, as well as the importance of apoptotic or necrotic pathways in symbiosis regulation will be vital to decipher the mechanisms underlying the breakdown of the *Cassiopea* symbiosis during heat stress.

Ecological relevance

While host shrinkage and in hospite symbiont degradation may have compensated for and delayed a visible bleaching response, the prolonged exposure to severe heat stress of 34 °C clearly exceeded the thermal tolerance of the *Cassiopea* holobiont in the present study. Thermal thresholds are species and context dependent, but the thermal upper limit measured in this study is consistent with previous reports [46–48]. Thus, while *Cassiopea* displayed signs of susceptibility to acute heat stress, their thermal tolerance likely exceeds that of most scleractinian corals [47, 86].

Our results suggest that the thermotolerance of *Cassiopea* depends in part on the nutritional status of the host. In our study, the mesoglea likely acted as an

important energy reserve that was gradually depleted, as suggested by the observed animal shrinkage during heat stress. As the mesoglea of scyphozoan jellyfish is substantially larger than that of most scleractinian corals, this additional energy reservoir likely supports the metabolic requirements of *Cassiopea* during heat stress and contributes to its higher heat tolerance. In addition, efficient heterotrophic feeding may enable *Cassiopea* to mitigate decreased translocation of photosynthates during heat stress. In our study, the absence of heterotrophic feeding likely lowered the thermotolerance of *Cassiopea* compared to in situ conditions. Although species-specific differences in thermotolerance likely exist [87], it is thus plausible that large energy reserves and a high heterotrophic capacity enable *Cassiopea* to thrive in changing, warming, and anthropogenically affected environments.

Future studies are thus needed to address the role of heterotrophic feeding in the heat stress response of *Cassiopea* and validate the observed responses under in situ conditions. In addition, the functional importance of prokaryotic members of the *Cassiopea* holobiont is poorly understood at this point. Efforts to address microbial contributions to nitrogen cycling, antioxidant production, or immune response in *Cassiopea* would also yield further insights into the high heat tolerance of these organisms.

Conclusion

While the bleaching phenotype of heat-stressed *Cassiopea* can differ from other photosymbiotic cnidarians, our results suggest that there are also important similarities with processes described in scleractinian corals and sea anemones [26, 88]. In particular, during heat stress, energy and carbon limitation of the host rapidly shifts the host metabolism to a net catabolic state in which the relative contribution of algal photosynthates to host nutrition is greatly reduced. Thus, our results reinforce the notion that *Cassiopea* represents a highly relevant laboratory model organism to study the metabolic response of photosymbiotic cnidarians facing heat stress. It also shows that host bioenergetic status represents a critical parameter shaping the heat stress response among symbiotic cnidarians.

In addition, the observed "invisible" bleaching phenomenon and relative heat tolerance of *Cassiopea* likely are a result of its unique anatomy and cellular organization. The larger mesoglea, in comparison to other photosymbiotic cnidarians, and the isolation of algal symbionts in the amoebocytes may represent an adaptive benefit contributing to *Cassiopea* ability to tolerate and spread in rapidly changing and extreme environments.

Supplementary Information

The online version contains supplementary material available at https://doi.org/10.1186/s40168-023-01738-0.

Additional file 1: Figure S1. Schematic presentation of the experimental setup viewed from the side and from above with sampling design information. **Figure S2.** Photos of the medusae collected at SP2 on day 1 and 10 of the experiment in the control treatment, and heat stress treatment. **Figure S3.** Impact of heat stress on chlorophyll a content and algal symbiont density per wet weight. **Figure S4.** Temperature effects on the enrichment from assimilation of isotopically labeled bicarbonate and ammonium in the epidermis of heat-stressed medusae. **Figure S5.** SEM and $^{12}C_2^-$ and $^{14}N^{12}C^-$ NanoSIMS images corresponding to the correlative SEM and NanoSIMS images presented in Fig. 3. **Figure S6.** Tissue and cellular ultrastructure of control and heat-stressed medusae bells at SP2 imaged by light microscopy with H&E staining and SEM. **Table S1.** Number of NanoSIMS images per biological replicate and the associated number of regions of interest (ROIs) per *Cassiopea* compartment defined for the isotopic enrichment analyses.

Availability of data and materials

All raw data associated with this study have been deposited in the zenodo.org repository: https://doi.org/https://doi.org/10.5281/zenodo.8020430.

Declarations

Ethics approval and consent to participate
Not applicable.

Consent for publication
All authors consent to the publication of the article.

Competing interests
The authors declare no competing interests.

Author details
[1]Laboratory for Biological Geochemistry, School of Architecture, Civil and Environmental Engineering, École Polytechnique Fédérale de Lausanne (EPFL), Lausanne 1015, Switzerland. [2]PSL Université Paris: EPHE-UPVD-CNRS, UAR 3278 CRIOBE, Université de Perpignan, 52 Avenue Paul Alduy, Perpignan Cedex 66860, France. [3]Electron Microscopy Facility, University of Lausanne, Lausanne 1015, Switzerland. [4]Center for Advanced Surface Analysis, Institute of Earth Science, University of Lausanne, Lausanne 1015, Switzerland. [5]Institute of Earth Surface Dynamics, University of Lausanne, Lausanne 1015, Switzerland.

References

1. Davy SK, Allemand D, Weis VM. Cell biology of cnidarian-dinoflagellate symbiosis. Microbiol Mol Biol Rev. 2012;76:229–61.
2. LaJeunesse TC, Parkinson JE, Gabrielson PW, Jeong HJ, Reimer JD, Voolstra CR, et al. Systematic revision of Symbiodiniaceae highlights the antiquity and diversity of coral endosymbionts. Curr Biol. 2018;28:2570–2580.e6.
3. Rädecker N, Meibom A. Symbiotic nutrient cycling enables the long-term survival of Aiptasia in the absence of heterotrophic food sources. Peer Commun J. 2023;3:e48
4. Falkowski PG, Dubinsky Z, Muscatine L, Porter JW. Light and the bioenergetics of a symbiotic coral. Bioscience. 1984;34:705–9.
5. Muscatine L, R. McCloskey L, E. Marian R. Estimating the daily contribution of carbon from zooxanthellae to coral animal respiration1. Limnol Oceanogr. 1981;26:601–11.
6. Freeman CJ, Stoner EW, Easson CG, Matterson KO, Baker DM. Symbiont carbon and nitrogen assimilation in the *Cassiopea-Symbiodinium* mutualism. Mar Ecol Prog Ser. 2016;544:281–6.
7. Kopp C, Domart-Coulon I, Escrig S, Humbel BM, Hignette M, Meibom A. Subcellular investigation of photosynthesis-driven carbon assimilation in the symbiotic reef coral *Pocillopora damicornis*. MBio. 2015;6:e02299–14
8. Cunning R, Muller EB, Gates RD, Nisbet RM. A dynamic bioenergetic model for coral-*Symbiodinium* symbioses and coral bleaching as an alternate stable state. J Theor Biol. 2017;431:49–62.
9. Leggat W, Badger MR, Yellowlees D. Evidence for an inorganic carbon-concentrating mechanism in the symbiotic dinoflagellate *Symbiodinium sp* Plant Physiol. 1999;121:1247–56.
10. Rädecker N, Pogoreutz C, Wild C. Stimulated respiration and net photosynthesis in *Cassiopeia sp.* during glucose enrichment suggests in hospite CO_2 limitation of algal endosymbionts. Front Marine. 2017;4:267.
11. Muscatine L, Porter JW. Reef corals: mutualistic symbioses adapted to nutrient-poor environments. Bioscience. 1977;27:454–60.
12. Hughes TP, Barnes ML, Bellwood DR, Cinner JE, Cumming GS, Jackson JBC, et al. Coral reefs in the Anthropocene. Nature. 2017;546:82–90.
13. Lesser MP. Oxidative stress causes coral bleaching during exposure to elevated temperatures. Coral Reefs. 1997;16:187–92.
14. Hughes TP, Kerry JT, Álvarez-Noriega M, Álvarez-Romero JG, Anderson KD, Baird AH, et al. Global warming and recurrent mass bleaching of corals. Nature. 2017;543:373–7.
15. Muscatine L, Porter JW, Kaplan IR. Resource partitioning by reef corals as determined from stable isotope composition. Mar Biol. 1989;100:185–93.
16. Frankowiak K, Wang XT, Sigman DM, Gothmann AM, Kitahara MV, Mazur M, et al. Photosymbiosis and the expansion of shallow-water corals. Sci Adv. 2016;2:e1601122.
17. Jones RJ, Hoegh-Guldberg O. Temperature-induced bleaching of corals begins with impairment of the CO_2 fixation mechanism in zooxanthellae. Plant Cell Environ. 1998;21:1219–30.
18. Hoegh-Guldberg O, Mumby PJ, Hooten AJ, Steneck RS, Greenfield P, Gomez E, et al. Coral reefs under rapid climate change and ocean acidification. Science. 2007;318:1737–42.
19. Hughes TP, Kerry JT, Baird AH, Connolly SR, Dietzel A, Eakin CM, et al. Global warming transforms coral reef assemblages. Nature. 2018;556:492–6.
20. Hoegh-Guldberg O. Climate change, coral bleaching and the future of the world's coral reefs. Ove Hoegh-Guldberg Mar Freshwater Res. 1999;50:839–66.
21. Ventura P, Toullec G, Fricano C, Chapron L, Meunier V, Röttinger E, et al. Cnidarian primary cell culture as a tool to investigate the effect of thermal stress at cellular level. Mar Biotechnol. 2018;20:144–54.
22. Bhagooli R, Hidaka M. Comparison of stress susceptibility of in hospite and isolated zooxanthellae among five coral species. J Exp Mar Bio Ecol. 2003;291:181–97.
23. Baker DM, Freeman CJ, Wong JCY, Fogel ML, Knowlton N. Climate change promotes parasitism in a coral symbiosis. ISME J. 2018;12:921–30.
24. Hoadley KD, Pettay DT, Grottoli AG, Cai W-J, Melman TF, Schoepf V, et al. Physiological response to elevated temperature and pCO2 varies across four Pacific coral species: understanding the unique host+symbiont response. Sci Rep. 2015;5:18371.
25. Gibbin EM, Krueger T, Putnam HM, Barott KL, Bodin J, Gates RD, et al. Short-term thermal acclimation modifies the metabolic condition of the coral holobiont. Front Mar Sci. 2018;5:10.
26. Rädecker N, Pogoreutz C, Gegner HM, Cárdenas A, Roth F, Bougoure J, et al. Heat stress destabilizes symbiotic nutrient cycling in corals. Proc Natl Acad Sci U S A. 2021;118:e2022653118.
27. Anthony KRN, Hoogenboom MO, Maynard JA, Grottoli AG, Middlebrook R. Energetics approach to predicting mortality risk from environmental stress: a case study of coral bleaching. Funct Ecol. 2009;23:539–50.
28. Tremblay P, Gori A, Maguer JF, Hoogenboom M, Ferrier-Pagès C. Heterotrophy promotes the re-establishment of photosynthate translocation in a symbiotic coral after heat stress. Sci Rep. 2016;6:38112.
29. Grottoli AG, Rodrigues LJ, Palardy JE. Heterotrophic plasticity and resilience in bleached corals. Nature. 2006;440:1186–9.
30. Lampert KP. *Cassiopea* and its zooxanthellae. In: Goffredo S, Dubinsky Z, editors. The Cnidaria, Past, Present and Future: The world of Medusa and her sisters. Cham: Springer International Publishing; 2016. p. 415–23.
31. Medina M, Sharp V, Ohdera A, Bellantuono A, Dalrymple J, Gamero-Mora E, et al. The upside-down jellyfish *Cassiopea xamachana* as an emerging model system to study cnidarian–algal symbiosis. Handbook of Marine Model Organisms in Experimental Biology. CRC Press; 2021. p. 149–71.
32. Ohdera AH, Abrams MJ, Ames CL, Baker DM, Suescún-Bolívar LP, Collins AG, et al. Upside-down but headed in the right direction: review of the highly versatile *Cassiopea xamachana* system. Front Ecol Evol. 2018;6:35.
33. Lyndby NH, Rädecker N, Bessette S, Søgaard Jensen LH, Escrig S, Trampe E, et al. Amoebocytes facilitate efficient carbon and nitrogen assimilation in the *Cassiopea*-Symbiodiniaceae symbiosis. Proc Biol Sci. 2020;287:20202393.
34. Colley NJ, Trench RK. Cellular events in the reestablishment of a symbiosis between a marine dinoflagellate and a coelenterate. Cell Tissue Res. 1985;239:93–103.
35. Cates N. Productivity and organic consumption in *Cassiopea* and *Condylactus*. J Exp Mar Bio Ecol. 1975;18:55–9.
36. Hofmann DK, Kremer BP. Carbon metabolism and strobilation in *Cassiopea andromedea* (Cnidaria: Scyphozoa): Significance of endosymbiotic dinoflagellates. Mar Biol. 1981;65:25–33.
37. Verde EA, McCloskey LR. Production, respiration, and photophysiology of the mangrove jellyfish *Cassiopea xamachana* symbiotic with zooxanthellae:effect of jellyfish size and season. Mar Ecol Prog Ser. 1998;168:147–62.
38. Hambleton EA, Jones VAS, Maegele I, Kvaskoff D, Sachsenheimer T, Guse A. Sterol transfer by atypical cholesterol-binding NPC2 proteins in coral-algal symbiosis. Elife. 2019;8:e43923.
39. Holland BS, Dawson MN, Crow GL, Hofmann DK. Global phylogeography of *Cassiopea* (Scyphozoa: Rhizostomeae): molecular evidence for cryptic species and multiple invasions of the Hawaiian Islands. Mar Biol. 2004;145:1119–28.
40. Morandini AC, Stampar SN, Maronna MM, Da Silveira FL. All non-indigenous species were introduced recently? the case study of *Cassiopea* (Cnidaria: Scyphozoa) in Brazilian waters. J Mar Biol Assoc U K. 2017;97:321–8.
41. Thé J, Gamero-Mora E, Chagas da Silva MV, Morandini AC, Rossi S, Soares M de O. Non-indigenous upside-down jellyfish *Cassiopea andromeda* in shrimp farms (Brazil). Aquaculture. 2021;532:735999.
42. Cillari T, Allegra A, Berto D, Bosch-Belmar M, Falautano M, Maggio T, et al. Snapshot of the distribution and biology of alien jellyfish *Cassiopea andromeda* (Forsskål, 1775) in a Mediterranean Touristic Harbour. Biology. 2022;11:319.
43. Purcell JE, Uye S, Lo W. Anthropogenic causes of jellyfish blooms and their direct consequences for humans: a review. Mar Ecol Prog Ser. 2007;350:153–74.
44. Aljbour SM, Zimmer M, Al-Horani FA, Kunzmann A. Metabolic and oxidative stress responses of the jellyfish Cassiopea sp. to changes in seawater temperature. J Sea Res. 2019;145:1–7.
45. Banha TNS, Mies M, Güth AZ, Pomory CM, Sumida PYG. Juvenile *Cassiopea andromeda* medusae are resistant to multiple thermal stress events. Mar Biol. 2020;167:173.
46. Béziat P, Kunzmann A. Under pressure: *Cassiopea andromeda* jellyfish exposed to increasing water temperature or lead, cadmium and anthropogenic gadolinium contamination. Mar Biol Res. 2022;18:48–63.

47. Klein SG, Pitt KA, Lucas CH, Hung S-H, Schmidt-Roach S, Aranda M, et al. Night-time temperature reprieves enhance the thermal tolerance of a symbiotic cnidarian. Front Mar Sci. 2019;6:453.
48. McGill CJ, Pomory CM. Effects of bleaching and nutrient supplementation on wet weight in the jellyfish *Cassiopea xamachana*(Bigelow) (Cnidaria: Scyphozoa). Mar Freshw Behav Physiol. 2008;41:179–89.
49. Tilstra A, El-Khaled YC, Meier S, Wild C. Invasive upside-down jellyfish tolerate organic eutrophication and warming. Bull Mar Sci. 2022;98:381–92.
50. Djeghri N, Pondaven P, Stibor H, Dawson MN. Review of the diversity, traits, and ecology of zooxanthellate jellyfishes. Mar Biol. 2019;166:147.
51. Mammone M, Ferrier-Pagés C, Lavorano S, Rizzo L, Piraino S, Rossi S. High photosynthetic plasticity may reinforce invasiveness of upside-down zooxanthellate jellyfish in Mediterranean coastal waters. PLoS ONE. 2021;16:e0248814.
52. Aljbour SM, Zimmer M, Kunzmann A. Cellular respiration, oxygen consumption, and trade-offs of the jellyfish *Cassiopea* sp. in response to temperature change. J Sea Res. 2017;128:92–7.
53. Purcell JE. Jellyfish and ctenophore blooms coincide with human proliferations and environmental perturbations. Ann Rev Mar Sci. 2012;4:209–35.
54. Spangenberg JE, Zufferey V. Changes in soil water availability in vineyards can be traced by the carbon and nitrogen isotope composition of dried wines. Sci Total Environ. 2018;635:178–87.
55. Hoppe P, Cohen S, Meibom A. NanoSIMS: technical aspects and applications in cosmochemistry and biological geochemistry. Geostand Geoanal Res. 2013;37:111–54.
56. Venables WN, Smith DM. R Developmental Core Team. An introduction to R Bristol: Network Theory Limited. 2001.
57. Morris LA, Voolstra CR, Quigley KM, Bourne DG, Bay LK. Nutrient availability and metabolism affect the stability of coral–symbiodiniaceae symbioses. Trends Microbiol. 2019;27:678–89.
58. Gillooly JF, Brown JH, West GB, Savage VM, Charnov EL. Effects of size and temperature on metabolic rate. Science. 2001;293:2248–51.
59. Nevarez-Lopez CA, Sanchez-Paz A, Lopez-Martinez J, Llera-Herrera R, Muhlia-Almazan A. Metabolic response of the cannonball jellyfish *Stomolophus meleagris* upon short-term exposure to thermal stress. J Sea Res. 2020;166:101959.
60. Fitt WK, Costley K. The role of temperature in survival of the polyp stage of the tropical rhizostome jellyfish *Cassiopea xamachana* J Exp Mar Bio Ecol. 1998;222:79–91.
61. Haunerland NH. Invertebrate Metabolism. eLS. Wiley; 2003.
62. Gardner EP, Zubkoff PL. Monomeric constituents of the mesogleal polysaccharides of *Chrysaora quinquecirrha* (scyphozoa: semaeostomeae). Compar Biochem Physiol Part B: Compar Biochem. 1978;61:161–3.
63. Pedersen MT, Vilgis TA. Soft matter physics meets the culinary arts: from polymers to jellyfish. Int J Gastron Food Sci. 2019;16:100135.
64. Chapman G. Studies on the Mesogloea of coelenterates. J Exper Biol. 1953:440–51.
65. Muffett KM, Aulgur J, Miglietta MP. Impacts of light and food availability on early development of *Cassiopea* Medusae. Front Mar Sci. 2022;8:783876.
66. Fu Z, Shibata M, Makabe R, Ikeda H, Uye S. Body size reduction under starvation, and the point of no return, in ephyrae of the moon jellyfish *Aurelia aurita* Mar Ecol Prog Ser. 2014;510:255–63.
67. Rädecker N, Raina J-B, Pernice M, Perna G, Guagliardo P, Kilburn MR, et al. Using Aiptasia as a model to study metabolic interactions in cnidarian-*Symbiodinium* symbioses. Front Physiol. 2018;9:214.
68. Cui G, Mi J, Moret A, Zhong H, Hung S-H, Al-Babili S, et al. Nitrogen competition is the general mechanism underlying cnidarian-Symbiodiniaceae symbioses. bioRxiv. 2022 [cited 2022 Nov 14]. p. 2022.06.30.498212.
69. Weis VM. Cellular mechanisms of Cnidarian bleaching: stress causes the collapse of symbiosis. J Exp Biol. 2008;211:3059–66.
70. Bieri T, Onishi M, Xiang T, Grossman AR, Pringle JR. Relative contributions of various cellular mechanisms to loss of algae during cnidarian bleaching. PLoS ONE. 2016;11:e0152693.
71. Franklin DJ, Hoegh-Guldberg O, Jones RJ, Berges JA. Cell death and degeneration in the symbiotic dinoflagellates of the coral *Stylophora pistillata* during bleaching. Mar Ecol Prog Ser. 2004;272:117–30.
72. Parisi MG, Parrinello D, Stabili L, Cammarata M. Cnidarian immunity and the repertoire of defense mechanisms in Anthozoans. Biology. 2020:283.
73. Fankboner PV. Intracellular digestion of symbiontic zooxanthellae by host amoebocytes in giant clams (Bivalvia: Tridacnidae), with a note on the nutritional role of the hypertrophied siphonal epidermis. Biol Bull. 1971;141:222–34.
74. Snyder GA, Eliachar S, Connelly MT, Talice S, Hadad U, Gershoni-Yahalom O, et al. Functional characterization of Hexacorallia phagocytic cells. Front Immunol. 2021;12:662803.
75. Olano CT, Bigger CH. Phagocytic activities of the gorgonian coral *Swiftia exserta* J Invertebr Pathol. 2000;76:176–84.
76. Vargas-Ángel B, Peters EC, Kramarsky-Winter E, Gilliam DS, Dodge RE. Cellular reactions to sedimentation and temperature stress in the Caribbean coral *Montastraea cavernosa* J Invertebr Pathol. 2007;95:140–5.
77. Palmer CV, Traylor-Knowles NG, Willis BL, Bythell JC. Corals use similar immune cells and wound-healing processes as those of higher organisms. PLoS ONE. 2011;6:e23992.
78. Mydlarz LD, Holthouse SF, Peters EC, Harvell CD. Cellular responses in sea fan corals: granular amoebocytes react to pathogen and climate stressors. PLoS ONE. 2008;3:e1811.
79. Downs CA, Kramarsky-Winter E, Martinez J, Kushmaro A, Woodley CM, Loya Y, et al. Symbiophagy as a cellular mechanism for coral bleaching. Autophagy. 2009;5:211–6.
80. Dunn SR, Bythell JC, Le Tissier MDA, Burnett WJ, Thomason JC. Programmed cell death and cell necrosis activity during hyperthermic stress-induced bleaching of the symbiotic sea anemone *Aiptasia sp* J Exp Mar Bio Ecol. 2002;272:29–53.
81. Dunn SR, Thomason JC, Le Tissier MDA, Bythell JC, Moosa MK, Others. Detection of cell death activity during experimentally induced bleaching of the symbiotic sea anemone *Aiptasia sp.* Proceedings of the Ninth International Coral Reef Symposium, Bali. 2000. p. 145–53.
82. Dunn SR, Thomason JC, Le Tissier MDA, Bythell JC. Heat stress induces different forms of cell death in sea anemones and their endosymbiotic algae depending on temperature and duration. Cell Death Differ. 2004;11:1213–22.
83. Dunn SR, Schnitzler CE, Weis VM. Apoptosis and autophagy as mechanisms of dinoflagellate symbiont release during cnidarian bleaching: every which way you lose. Proc Biol Sci. 2007;274:3079–85.
84. Sammarco PW, Strychar KB. Responses to high seawater temperatures in zooxanthellate octocorals. PLoS ONE. 2013;8:e54989.
85. Paxton CW, Davy SK, Weis VM. Stress and death of cnidarian host cells play a role in cnidarian bleaching. J Exp Biol. 2013;216:2813–20.
86. Fitt W, Brown B, Warner M, Dunne R. Coral bleaching: interpretation of thermal tolerance limits and thermal thresholds in tropical corals. Coral Reefs. 2001;51–65.
87. Fitt WK, Hofmann DK, Kemp DW, Ohdera AH. Different physiology in the jellyfish *Cassiopea xamachana* and *C. frondosa* in Florida Bay. Oceans (Basel). 2021;2:811–21.
88. Cziesielski MJ, Liew YJ, Cui G, Aranda M. Increased incompatibility of heterologous algal symbionts under thermal stress in the cnidarian-dinoflagellate model Aiptasia. Commun Biol. 2022;5:760.

Publisher's Note